EARTHQUAKE ENGINEERING AND STRUCTURAL DYNAMICS
Earthquake Engng. Struct. Dyn. **28**, 565–584 (1999)

AMPLIFICATION OF WAVES BY AN ORTHOTROPIC BASIN: SAGITTAL PLANE MOTION

TAO ZHENG AND MARIJAN DRAVINSKI *

Department of Mechanical Engineering, University of Southern California, Los Angeles, CA 90089-1453, U.S.A.

SUMMARY

Scattering of elastic waves by an orthotropic basin of arbitrary shape embedded in a half-space is investigated for the sagittal plane motion using an indirect boundary integral equation approach. Steady-state results were obtained for incident plane harmonic pseudo P-, S-, and Rayleigh waves. Detailed convergence analysis of the method is presented. Green's functions are evaluated by using adaptive Newton–Cotes or Filon quadratures. Surface ground motion is presented for semicircular and semielliptical basins with different material properties and various angles of incidence. The results show that surface motion strongly depends upon nature of incident wave, geometry and material properties of the basin, and location of the observation point. Comparison with isotropic basin response demonstrates that anisotropy is very important in amplification of surface ground motion. Copyright © 1999 John Wiley & Sons, Ltd.

KEY WORDS: anisotropic basin; site response

1. INTRODUCTION

Scattering of elastic waves by isotropic subsurface inclusions has been the subject of many studies in non-destructive evaluation of materials and prediction of earthquake induced ground motion atop a sediment-filled valley (e.g. References 1 and 2). For example, for amplification of elastic waves by two- and three-dimensional isotropic alluvial valleys, an extensive literature review can be found in the paper by Bouchon and Coutant.[2] These studies provided reasonable understanding of the site amplification for isotropic models. For general anisotropic media studies detailed survey of literature can be found in Nayfeh.[3] As for the scattering of elastic waves problems Rajapakse and Gross[4] examined the response of an orthotropic elastic medium with an embedded cavity of arbitrary shape due to transient pressurization using a boundary integral equation method. Karabulut and Ferguson[5] studied SH-wave propagation in transversely isotropic medium by using discrete wavenumber boundary integral method. Two semi-infinite half-spaces and a multi-layered earth model were considered.

Recently, Zheng and Dravinski[6] considered amplification of SH-waves by an orthotropic basin of arbitrary shape using an indirect boundary integral equation method. The antiplane strain results showed that material anisotropy may significantly change surface response of a basin when

* Correspondence to: Marijan Dravinski, Department of Mechanical Engineering, Olin Hall 430, University of Southern California, Los Angeles, CA 90089-1453, U.S.A. E-mail: mdravins@mizar.usc.edu

CCC 0098–8847/99/060565–20$17·50

Received 27 January 1998
Revised 23 July 1998

compared with the corresponding isotropic model. Present paper is a continuation of that investigation to include the motion in the sagittal plane.

Problem of diffraction of elastic waves by an obstacle embedded within an elastic medium can be solved analytically or numerically. The analytical solutions apply mainly to linear, isotropic, and homogeneous materials, and simple geometries. The numerical solutions, on the other hand, are often inapplicable to the problems of interest in earthquake engineering and strong ground motion seismology. Namely, the most commonly used numerical methods, finite elements and finite differences, require a construction of a computational grid which fills the solution domain of the problem in space and time. This reduces the effectiveness of these methods for geotechnical problems which involve large dimensions. In addition, for finite element and finite difference methods the radiation conditions in the far field are not satisfied exactly.[7]

Boundary Element Methods (BEM) are efficient techniques for modelling unbounded media since they require discretization only along the boundaries of the model and the radiation in the far field is satisfied exactly.[8] Boundary integral equation methods can be of direct or indirect type. Direct methods require calculation of the displacement Green's functions and their spatial derivatives. For indirect methods, only the displacement Green's functions need to be computed but care must be taken for the placement of the auxiliary surfaces.

The indirect boundary integral equation method used in this paper originates in the works of Ursell[9] and Kupradze.[10] Extensions of the method to the wave propagation problems in geophysics and earthquake engineering can be found in papers by Sanchez-Sesma and Rosenblueth,[11] Wong[12] and Dravinski.[13]

2. STATEMENT OF PROBLEM

The objective of this paper is to determine the elastodynamic field generated by incident plane waves of different types in an orthotropic basin perfectly embedded within a half-space. Geometry of the problem is depicted by Figure 1. The model consists of a half-space with a sedimentary basin of arbitrary shape. The interface C between the basin and the half-space is assumed to be sufficiently smooth without any corners. The domains of the half-space and the basin are denoted by D_1 and D_2, respectively. Materials are assumed to be linearly elastic, homogeneous, and orthotropic with the symmetry planes coincident with the Cartesian co-ordinate system $x_i,\ i=1,2,3$.

The equations of motion for a general anisotropic medium without body forces are given by[3]

$$\sigma_{ij,j}+\rho\omega^2 u_i=0; \qquad (\bullet)_{,j}\equiv\partial(\bullet)/\partial x_j, \quad i,j=1,2,3 \tag{1}$$

where ρ is the mass density, $\sigma_{ij}(\mathbf{x},\omega)$, and $u_i(\mathbf{x},\omega)$, are, respectively, the components of stress and displacement, while ω denotes circular frequency. Unless stated differently, summation over repeated indices is understood. Throughout, the time dependence factor $e^{-\sqrt{-1}\omega t}$ is understood.

It should be noted that if the co-ordinate system is chosen to be in arbitrary direction then the material behaves as those with lower symmetry and the problem becomes more complicated. However at this stage of investigation the simplest case is considered in order to determine the influence of material anisotropy on the surface response.

The stress–strain relations for a homogeneous anisotropic linearly elastic solid are given by the generalized Hooke's law,

$$\sigma_{ij}=c_{ijkl}e_{kl}, \quad i,j,k,l=1,2,3 \tag{2}$$

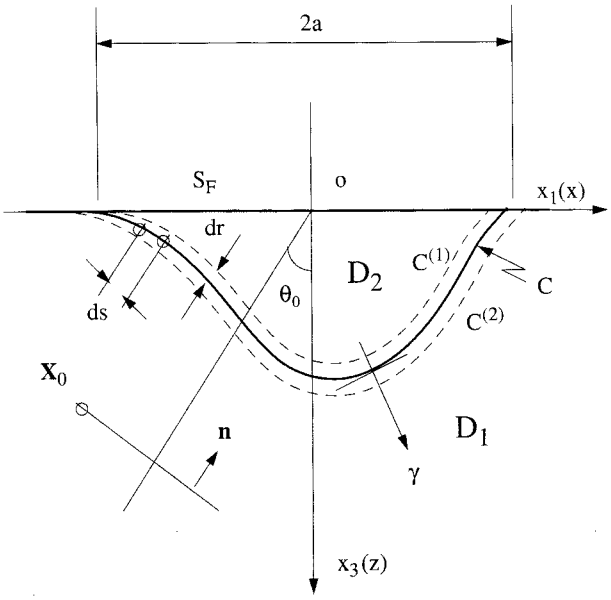

Figure 1. Problem model

where $e_{kl}(\mathbf{x},\omega)$ are strain components defined by

$$e_{kl} = \tfrac{1}{2}(u_{k,l} + u_{l,k}) \tag{3}$$

In equation (2) c_{ijkl} are the constants of elasticity. By virtue of the symmetry conditions

$$c_{ijkl} = c_{jikl} = c_{ijlk} = c_{klij} \tag{4}$$

out of 81 components of c_{ijkl} only 21 are independent. In particular, for an orthotropic material, the constitutive equations can be written as[3]

$$\begin{bmatrix} \sigma_{11} \\ \sigma_{22} \\ \sigma_{33} \\ \sigma_{23} \\ \sigma_{13} \\ \sigma_{12} \end{bmatrix} = \begin{bmatrix} C_{11} & C_{12} & C_{13} & 0 & 0 & 0 \\ C_{12} & C_{22} & C_{23} & 0 & 0 & 0 \\ C_{13} & C_{23} & C_{33} & 0 & 0 & 0 \\ 0 & 0 & 0 & C_{44} & 0 & 0 \\ 0 & 0 & 0 & 0 & C_{55} & 0 \\ 0 & 0 & 0 & 0 & 0 & C_{66} \end{bmatrix} \begin{bmatrix} e_{11} \\ e_{22} \\ e_{33} \\ \gamma_{23} \\ \gamma_{13} \\ \gamma_{12} \end{bmatrix} \tag{5}$$

where $\gamma_{ij} = 2e_{ij}$ (with $i \neq j$) represents the engineering shear components. In order to relate c_{ijkl} to C_{pq} $(i,j,k,l = 1,2,3$ and $p,q = 1,2,\ldots,6)$ the following subscript contracting convention has been used: $1 \to 11, 2 \to 22, 3 \to 33, 4 \to 23, 5 \to 13$, and $6 \to 12$. Thus, for example, $c_{1122} \to C_{12}$ and so on.

Substituting equation (5) into equation (1) results in the following partial differential equations for the displacement components u_1, u_2 and u_3:

$$C_{11}u_{1,11} + C_{55}u_{1,33} + (C_{13} + C_{55})u_{3,13} + \rho\omega^2 u_1 = 0 \tag{6}$$

$$C_{66}u_{2,11} + C_{44}u_{2,33} + \rho\omega^2 u_2 = 0 \tag{7}$$

$$(C_{13} + C_{55})u_{1,13} + C_{55}u_{3,11} + C_{33}u_{3,33} + \rho\omega^2 u_3 = 0 \tag{8}$$

Therefore, the equations of motion are partially decoupled. Equation (7) governs the SH-motion while equations (6) and (8) correspond to the motion in the sagittal plane. Thus the displacement field vector considered in this paper involve only two components, i.e. $\mathbf{u} = (u_1, 0, u_3)$.

The stress-free boundary conditions are given by

$$\sigma_{13}^{(j)} = \sigma_{33}^{(j)} = 0, \quad x_3 = 0, \ \mathbf{x} \in D_j, \ j = 1, 2 \tag{9}$$

where the superscript (j) denotes the domain D_j. Perfect bonding along the interface C between the half-space and the basin can be stated as

$$\begin{aligned} (u_1, 0, u_3)^{(1)} &= (u_1, 0, u_3)^{(2)}, \quad \mathbf{x} \in C \\ (t_1, 0, t_3)^{(1)} &= (t_1, 0, t_3)^{(2)}, \quad \mathbf{x} \in C \end{aligned} \tag{10}$$

where $t_i = \sigma_{ij}\gamma_j$ are components of the traction vector and $\boldsymbol{\gamma}$ denotes unit normal vector on C (see Figure 1).

As an incident wave strikes the basin it generates scattered waves. These interact with the free-field resulting in amplification (constructive interference) or reduction (destructive interference) of motion. The objective of this paper is to determine the unknown scattered waves and subsequently the displacement and stress fields throughout the medium.

3. SOLUTION OF PROBLEM

3.1. Free-field

Throughout the paper the incident wave will be assumed to be propagating upwards in the third quadrant (see Figure 1). Therefore, following the development of Nayfeh,[3] the general incident and reflected waves are represented by (see Appendix I)

$$\begin{aligned} (u_1, 0, u_3)^{\mathrm{i}} &= \sum_{q=2,4} (1, 0, W_q) U_{1q}^{\mathrm{i}} \mathrm{e}^{\sqrt{-1}k_1(x_1 + \alpha_q x_3 - ct)} \\ (u_1, 0, u_3)^{\mathrm{r}} &= \sum_{q=1,3} (1, 0, W_q) U_{1q}^{\mathrm{r}} \mathrm{e}^{\sqrt{-1}k_1(x_1 + \alpha_q x_3 - ct)} \end{aligned} \tag{11}$$

where U_{1q}^{i} are known and U_{1q}^{r} are to be determined. Here, W_q denotes the polarization directions, α_q defines the directions of propagation, and c represents apparent phase velocity along the surface of the half-space. Corresponding traction vectors are given by

$$\begin{aligned} (t_1, 0, t_3)^{\mathrm{i}} &= (\sigma_{1j}\gamma_j, 0, \sigma_{3j}\gamma_j)^{\mathrm{i}} \\ (t_1, 0, t_3)^{\mathrm{r}} &= (\sigma_{1j}\gamma_j, 0, \sigma_{3j}\gamma_j)^{\mathrm{r}} \end{aligned} \tag{12}$$

where

$$\begin{aligned} (\sigma_{13}, \sigma_{11}, \sigma_{33})^{\mathrm{i}} &= \sum_{q=2,4} \sqrt{-1}k_1 (D_{3q}, D_{2q}, D_{1q}) U_{1q}^{\mathrm{i}} \mathrm{e}^{\sqrt{-1}k_1(x_1 + \alpha_q x_3 - ct)} \\ (\sigma_{13}, \sigma_{11}, \sigma_{33})^{\mathrm{r}} &= \sum_{q=1,3} \sqrt{-1}k_1 (D_{3q}, D_{2q}, D_{1q}) U_{1q}^{\mathrm{r}} \mathrm{e}^{\sqrt{-1}k_1(x_1 + \alpha_q x_3 - ct)} \end{aligned} \tag{13}$$

and D_{1q}, D_{2q}, and D_{3q} are given in Appendix I.

The free-field can be written as

$$\begin{aligned}(u_1,0,u_3)^{\mathrm{ff}} &= (u_1,0,u_3)^{\mathrm{i}} + (u_1,0,u_3)^{\mathrm{r}} \\ (t_1,0,t_3)^{\mathrm{ff}} &= (t_1,0,t_3)^{\mathrm{i}} + (t_1,0,t_3)^{\mathrm{r}}\end{aligned} \tag{14}$$

Stress-free boundary conditions along the surface of the half-space for the free-field result in the following equation:

$$\begin{bmatrix} D_{11} & D_{13} \\ D_{31} & D_{33} \end{bmatrix} \begin{bmatrix} U_{11}^{\mathrm{r}} \\ U_{13}^{\mathrm{r}} \end{bmatrix} = \begin{bmatrix} -D_{11} & -D_{13} \\ D_{31} & D_{33} \end{bmatrix} \begin{bmatrix} U_{12}^{\mathrm{i}} \\ U_{14}^{\mathrm{i}} \end{bmatrix} \tag{15}$$

where it has been used that

$$\begin{aligned} D_{12} &= D_{11}, \quad D_{14} = D_{13} \\ D_{32} &= -D_{31}, \quad D_{34} = -D_{33} \end{aligned} \tag{16}$$

Equation (15) can be solved for the unknown reflected wave amplitudes. This topic is discussed next for three different incident waves.

3.1.1. Incident pseudo P-wave. In this case $U_{14}^{\mathrm{i}} = 0$ and the incident wave follows from equation (11) to be

$$(u_1,0,u_3)^{\mathrm{i}} = (1,0,W_2)U_{12}^{\mathrm{i}} \mathrm{e}^{\sqrt{-1}k_1(x_1+\alpha_2 x_3 - ct)} \tag{17}$$

Corresponding reflected waves are described by the bottom equation (11) with the unknown amplitudes determined from equation (15) to be

$$\begin{aligned} U_{11}^{\mathrm{r}} &= \frac{D_{11}D_{33} + D_{13}D_{31}}{D_{13}D_{31} - D_{11}D_{33}} U_{12}^{\mathrm{i}} \\ U_{13}^{\mathrm{r}} &= \frac{-2D_{11}D_{31}}{D_{13}D_{31} - D_{11}D_{33}} U_{12}^{\mathrm{i}} \end{aligned} \tag{18}$$

3.1.2. Incident pseudo S-wave. With $U_{12}^{\mathrm{i}} = 0$ the incident wave field becomes

$$(u_1,0,u_3)^{\mathrm{i}} = (1,0,W_4)U_{14}^{\mathrm{i}} \mathrm{e}^{\sqrt{-1}k_1(x_1+\alpha_4 x_3 - ct)} \tag{19}$$

and the amplitudes of the reflected waves are given by

$$\begin{aligned} U_{11}^{\mathrm{r}} &= \frac{2D_{13}D_{33}}{D_{13}D_{31} - D_{11}D_{33}} U_{14}^{\mathrm{i}} \\ U_{13}^{\mathrm{r}} &= -\frac{D_{13}D_{31} + D_{11}D_{33}}{D_{13}D_{31} - D_{11}D_{33}} U_{14}^{\mathrm{i}} \end{aligned} \tag{20}$$

3.1.3. Incident pseudo Rayleigh wave. Here the outgoing wave field is of the form

$$(u_1,0,u_3)^{\mathrm{R}} = \sum_{q=1,3} (1,0,W_q)U_{1q}^{\mathrm{R}} \mathrm{e}^{\sqrt{-1}k_1(x_1+\alpha_q x_3 - ct)} \tag{21}$$

and the stress-free boundary conditions along the surface of the half-space lead to

$$D_{11}D_{33} - D_{31}D_{13} = 0 \tag{22}$$

which defines the surface wave speed $c = c_R$. Based on this phase velocity one can solve for the directions of propagation $\alpha_{1,3}$ (see equation (56) in Appendix I). Furthermore, the boundary condition $\sigma_{33}(x_1, 0, 0) = 0$ implies that

$$U_{13}^R = -\frac{D_{11}}{D_{13}} U_{11}^R \tag{23}$$

Consequently, the displacement field specified by equation (21) can be expressed in terms of single displacement amplitude, say, U_{11}^R. The corresponding stress field then can be obtained in a straightforward manner.

If the material of the medium is assumed to be isotropic, the free-field results derived for pseudo P-, S-, and Rayleigh waves reduce to standard results for isotropic media.

This concludes the analysis of the free-field. The scattered waves are considered next.

3.2. *Scattered wave field*

As the incident wave strikes the interface C (Figure 1), it is partially transmitted into the basin and partially reflected into the half-space. Consequently, the waves in the half-space consist of the free- and the scattered wave fields, while the waves inside the basin comprise of scattered waves only. The displacement vectors in the half-space and the basin can be expressed as

$$\begin{aligned} (u_1, 0, u_3)^{(1)} &= (u_1, 0, u_3)^{\mathrm{ff}} + (u_1, 0, u_3)^{(1)\mathrm{s}}, \quad \mathbf{x} \in D_1 \\ (u_1, 0, u_3)^{(2)} &= (u_1, 0, u_3)^{(2)\mathrm{s}}, \quad \mathbf{x} \in D_2 \end{aligned} \tag{24}$$

where the superscripts s and ff denote the scattered and free-field, respectively.

Assuming that the scattered wave field can be expressed in terms of single layer potentials,[6, 9, 13] it means that the scattered fields in the half-space and the basin are obtained as a superposition of the responses to the corresponding line sources. This leads to

$$u_i^{(j)\mathrm{s}}(\mathbf{x}, \omega) = \int_{C^{(j)}} q_k^{(j)}(\mathbf{y}) G_{ik}^{(j)}(\mathbf{x}, \mathbf{y}, \omega)\, \mathrm{d}S(\mathbf{y}), \quad i, k = 1, 3, \ \ \mathbf{x} \in D_j, \ \ j = 1, 2 \tag{25}$$

Here $q_k^{(j)}$, $k = 1, 3$, are unknown density functions and $C^{(1)}$ and $C^{(2)}$ denote the auxiliary surfaces defined inside and outside of the interface C (Figure 1). $G_{ik}^{(j)}(\mathbf{x}, \mathbf{y}, \omega)$ are the half-space Green's functions which must satisfy the equations

$$\begin{aligned} c_{ijkl} G_{kp,jl} + \rho\omega^2 G_{ip} &= -\delta_{ip}\delta(\mathbf{x} - \mathbf{y}), \quad p = 1, 3 \\ \mathbf{x} &= (x_1, 0, x_3), \quad \mathbf{y} = (y_1, 0, y_3) \end{aligned} \tag{26}$$

and stress-free conditions at the surface of the half-space. Thus $G_{kp}(\mathbf{x}, \mathbf{y}, \omega)$ corresponds to the outgoing waves and it represents the kth component of displacement vector at $\mathbf{x}$ due to a harmonic load in the x_p-direction applied at $\mathbf{y}$. The corresponding stress field, $\sum_{ijp}$, may be determined

through the use of equation (2):

$$\sum_{ijp}(\mathbf{x},\mathbf{y},\omega)=c_{ijkl}G_{kp,l}(\mathbf{x},\mathbf{y},\omega) \tag{27}$$

The displacement and stress Green's functions are given by Rajapakse and Wang.[14]

If the scattered waves are assumed to be represented in terms of discrete line sources, equation (25) becomes

$$\begin{aligned}
u_1^{(1)s} &= a_m G_{11}^{(1)}(\mathbf{x},\mathbf{x}_m)+b_m G_{13}^{(1)}(\mathbf{x},\mathbf{x}_m), \quad \mathbf{x}_m\in C^{(1)}\\
u_3^{(1)s} &= a_m G_{31}^{(1)}(\mathbf{x},\mathbf{x}_m)+b_m G_{33}^{(1)}(\mathbf{x},\mathbf{x}_m), \quad \mathbf{x}_m\in C^{(1)}\\
m &= 1,\ldots,M\\
u_1^{(2)s} &= c_l G_{11}^{(2)}(\mathbf{x},\mathbf{x}_l)+d_l G_{13}^{(2)}(\mathbf{x},\mathbf{x}_l), \quad \mathbf{x}_l\in C^{(2)}\\
u_3^{(2)s} &= c_l G_{31}^{(2)}(\mathbf{x},\mathbf{x}_l)+d_l G_{33}^{(2)}(\mathbf{x},\mathbf{x}_l), \quad \mathbf{x}_l\in C^{(2)}\\
l &= 1,\ldots,L
\end{aligned} \tag{28}$$

where a_m, b_m, c_l, and d_l are unknown source intensities and summation over repeated indices m and l is understood.

Substitution of scattered wave (28) into equation (24) and then using the continuity conditions (10) leads to the following system of equations

$$\mathbf{A}\mathbf{a}=\mathbf{f} \tag{29}$$

The $4N$-by-$2(M+L)$ matrix $\mathbf{A}$ and $4N$-vector $\mathbf{f}$ are known (see Appendix II) while the $2(M+L)$-vector $\mathbf{a}^{\mathrm{T}}=[a_1,\ldots,a_M,b_1,\ldots,b_M,c_1,\ldots,c_L,d_1,\ldots,d_L]$ contains the unknown source intensities. Equation (29) is solved in the least-square sense using QR decomposition.[15] Once the source magnitudes are known, the scattered wave field can be determined according to equation (28).

This completes the solution of the problem. Numerical results are considered next.

4. NUMERICAL RESULTS

4.1. Evaluation of Green's functions

A typical integral in the numerical calculation of Green's functions is of the type

$$I=\int_0^\infty Q(\xi,z,z',\omega)\begin{Bmatrix}\cos(\delta x\xi)\\ \sin(\delta x\xi)\end{Bmatrix}\mathrm{d}\xi \tag{30}$$

where

$$\delta=\frac{\rho\omega^2}{C_{55}}, \quad z=x_3, \quad z'=y_3, \quad x=x_1$$

These integrals can be evaluated numerically provided that the problems which arise from very slow decay and the oscillatory nature of the integrand when $z\to z'$ are eliminated (source and observation points are at the same depth). It can be shown[4] that the function Q in equation

(30) behaves asymptotically as $e^{-\xi|z-z'|}$ and $1/\xi e^{-\xi|z-z'|}$ in the case of traction and displacement Green's functions, respectively. Consequently, direct integration for the displacement Green's function can be performed when $z \to z'$, but not for the traction Green's functions. For that purpose one can use the procedure originally suggested by Luco[16] and also used by Rajapakse and Wang.[4] In this approach the integral given by equation (30) is replaced by

$$I = \int_0^\infty [Q(\xi, z, z', \omega) - Q^*(\xi, z, z')] \begin{Bmatrix} \cos(\delta x \xi) \\ \sin(\delta x \xi) \end{Bmatrix} d\xi + I^* \tag{31}$$

where Q^* asymptotic value of Q for large ξ and

$$I^* = \int_0^\infty Q^*(\xi, z, z') \begin{Bmatrix} \cos(\delta x \xi) \\ \sin(\delta x \xi) \end{Bmatrix} d\xi \tag{32}$$

The first improper integral in equation (31) can be evaluated by a numerical quadrature and I^* can be determined analytically. In the present paper the integrals are calculated by using an adaptive Newton–Cotes quadrature as suggested by Van Loan[17] or an adaptive Filon quadrature.[18] All calculations were performed in a MATLAB environment which facilitates efficient vectorization of the algorithms.

4.2. *Verification of Green's functions*

In order to verify the algorithms used for numerical evaluation of Green's functions the problem of an orthotropic half-space loaded uniformly over a width of dimension $2a$ with intensity q_0 and acting at a depth $z'/a = 1$ is considered. For this problem, Rajapakse and Wang[14] calculated the Green's functions for three materials: ice, layered soil and Cadmium. Here, these calculations are reproduced together with the ones obtained in the present investigation. Calculations are done first by using adaptive Newton–Cotes quadrature and then repeated by using adaptive Filon integration rule. For the sake of briefness only two comparison results are shown here.

Figures 2 and 3 depict the Green's functions for ice and layered soil, respectively as a function of depth. Although some differences can be observed between the two calculations still, the results of Figures 2 and 3 confirm the accuracy of the proposed algorithms used for evaluation of Green's functions.

4.3. *Models*

Three models will be employed in the analysis of numerical results:

Model 1 consists of a semicircular isotropic basin of unit radius embedded within an isotropic half-space. In that case the material constants reduce to $C_{11} = C_{33} = \lambda + 2\mu$; $C_{13} = \lambda$ and $C_{55} = \mu$. Model 2 consists of a semi-circular orthotropic basin of unit radius while model 3 describes semi-elliptic orthotropic basin with the same material properties as in model 2. The principal axes for model 3 are assumed to be $R_1 = 1$ and $R_3 = 0{\cdot}7$. The material properties of the three models are described in Table I.

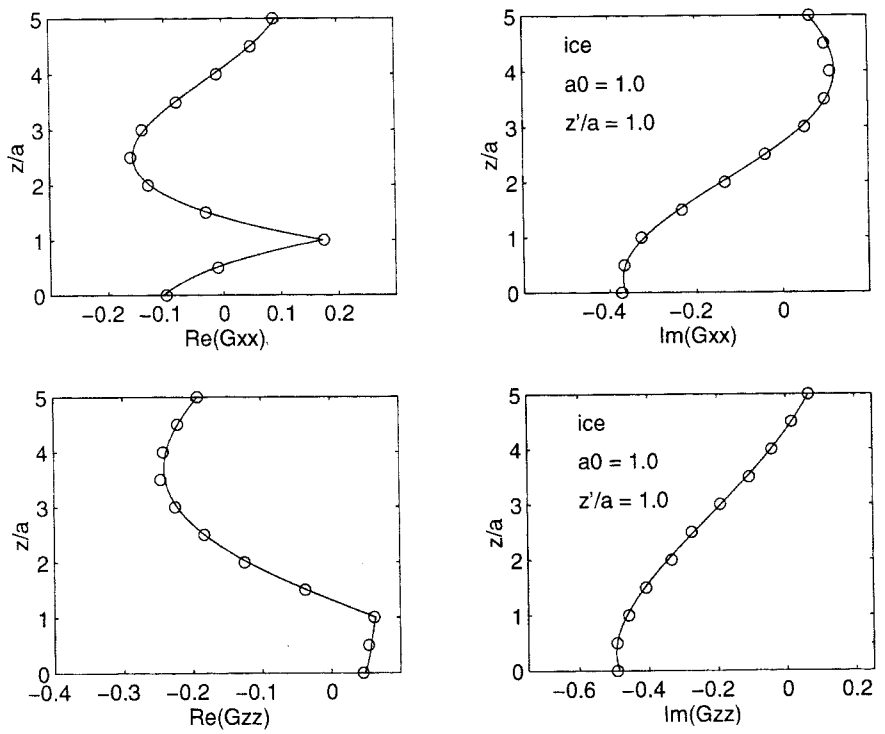

Figure 2. Testing of Green's functions for an othotropic half-space subjected to a distributed loading over a width $2a$ of intensity q_0 acting at a depth $z'/a = 1$. Normalized displacement Green's functions $G_{ij}C_{44}/(aq_0)$ are presented as functions of depth and frequency. Dimensionless frequency is defined by $a_0 = a\omega\sqrt{\rho/C_{44}} = 1$. Solid lines depict the results of this study while open circles those of Rajapakse and Wang.[14] The material properties for ice are assumed to be: $C_{11}/C_{55} = 4{\cdot}26, C_{12}/C_{55} = 2{\cdot}05,\ C_{33}/C_{55} = 4{\cdot}57, C_{13}/C_{55} = 1{\cdot}64, C_{55} = 0{\cdot}317 \times 10^4\ \mathrm{N/mm^2}$

4.4. *Testing and convergence analysis*

The indirect boundary integral equation method requires the following parameters (Figure 1)

- N—number of collocation points along the interface C between the half-space and the basin,
- M, L—number of source points along the auxiliary surfaces $C^{(1)}$ and $C^{(2)}$, respectively, and
- $\mathrm{d}r$—spacing between the auxiliary surfaces $C^{(1)}$, $C^{(2)}$ and the interface C.

The following relationships were suggested by Ding and Dravinski[19]

$$\mathrm{d}s < \frac{1}{10}\lambda^{\mathrm{inc}} \tag{33}$$

$$\mathrm{d}r \simeq 3\mathrm{d}s \tag{34}$$

$$\frac{2N}{M+L} = 2{\cdot}25 \sim 4{\cdot}0 \tag{35}$$

$$M = L \tag{36}$$

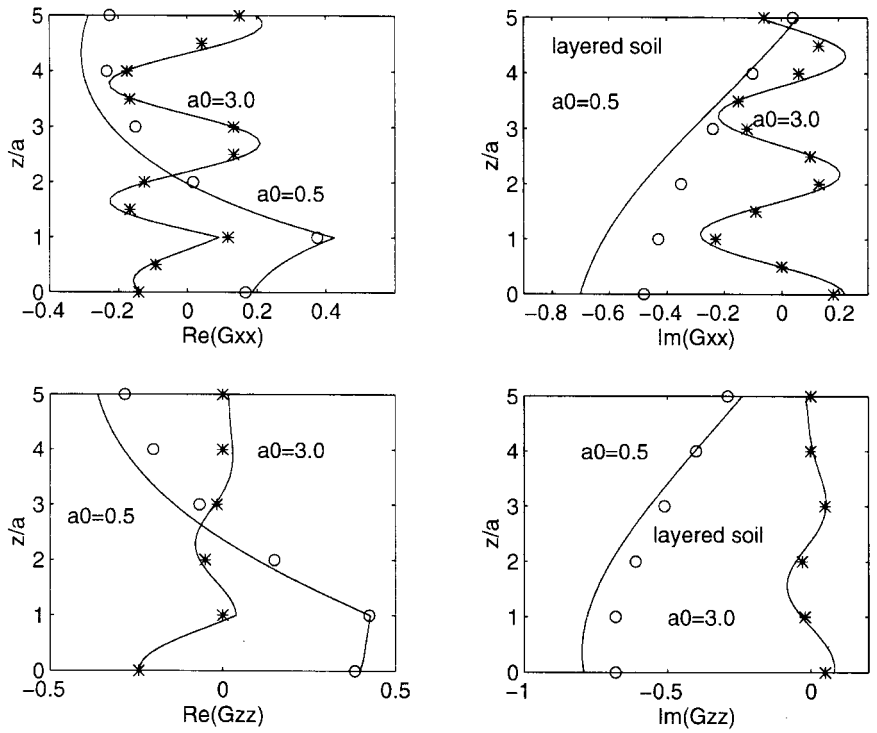

Figure 3. The same as in Figure 2 for layered soil and frequencies $a_0 = 0{\cdot}5$ and 3. Material properties are assumed to be: $C_{11}/C_{55} = 2{\cdot}11, C_{12}/C_{55} = 0{\cdot}43, C_{33}/C_{55} = 2{\cdot}58, C_{13}/C_{55} = 0{\cdot}47, C_{55} = 1{\cdot}40 \times 10^4$ N/mm^2

Table I. Material properties for three models

Model 1:	$\mu^{(1)}$	$\beta^{(1)}$	$\alpha^{(1)}$	$\mu^{(2)}$	$\beta^{(2)}$	$\alpha^{(2)}$
	1	1	2	1/6	1/2	1
Models 2,3:	$C_{11}^{(1)}/C_{55}^{(1)}$	$C_{13}^{(1)}/C_{55}^{(1)}$	$C_{33}^{(1)}/C_{55}^{(1)}$	$C_{55}^{(1)}$	$\rho^{(1)}$	
	3·9	1·8	5·1	1	1·5	
	$C_{11}^{(2)}/C_{55}^{(2)}$	$C_{13}^{(2)}/C_{55}^{(2)}$	$C_{33}^{(2)}/C_{55}^{(2)}$	$C_{55}^{(2)}$	$\rho^{(2)}$	
	0·65	0·3	0·85	0·1667	1	

where ds denotes the spacing between two adjacent collocation points and λ^{inc} is the incident wave length.

The basin interface C is specified by

$$\begin{aligned} x &= R_1 \cos\theta \\ z &= R_3 \sin\theta, \quad 0 \leqslant \theta \leqslant \pi \end{aligned} \tag{37}$$

where R_1 and R_3 denote the major and minor principal axes, respectively.

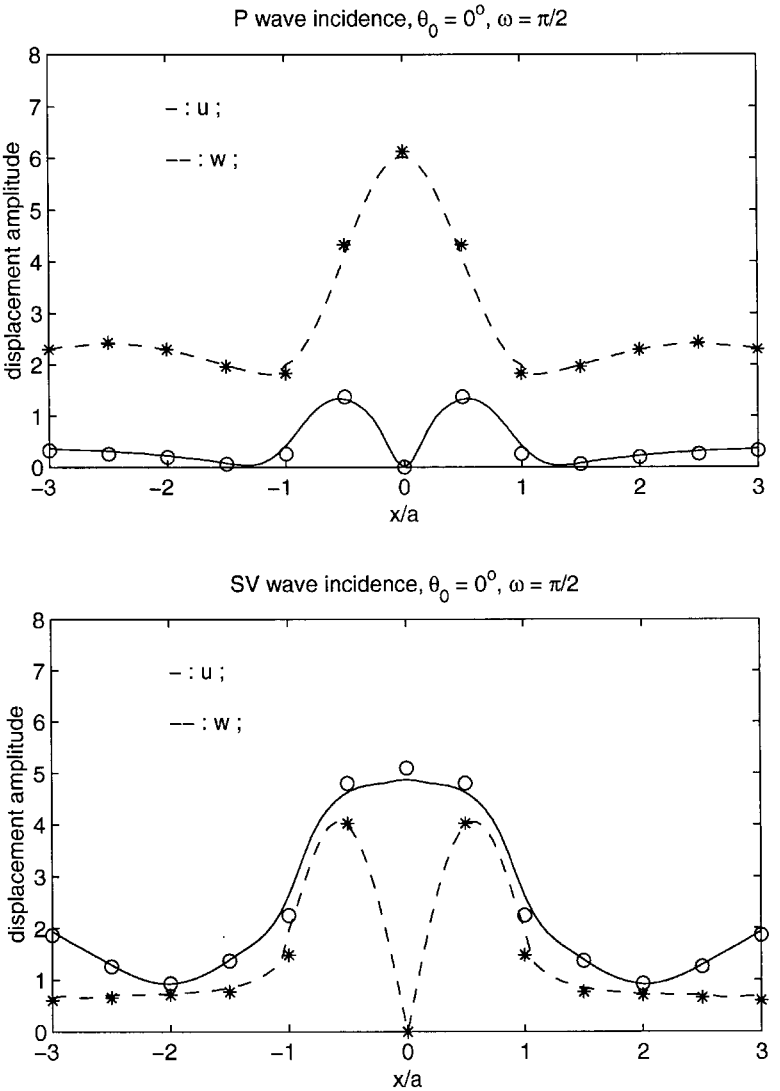

Figure 4. Test for surface response of an isotropic semi-circular basin of unit radius subjected to a vertically incident P-wave (top) and SV-wave ($u = u_1$ and $w = u_3$). Solid and dash lines denote the results obtained in this study while stars and open circles correspond to those of Dravinski and Mossessian.[7] Material properties: $C_{11} = C_{22} = C_{33} = \lambda + 2\mu$; $C_{12} = C_{13} = C_{23} = \lambda$; $C_{44} = C_{55} = C_{66} = \mu$. $\mu_1 = \beta_1 = \sqrt{\mu/\rho} = 1$; $\alpha_1 = \sqrt{(\lambda + 2\mu)/\rho} = 2$; $\nu_1 = 1/3$; $\rho_1 = 1$; $\mu_2 = 1/6$; $\beta_2 = 1/2$; $\alpha_2 = 1$; $\nu_2 = 1/3$; $\rho_2 = 2/3$; $\omega = \pi/2\,\mathrm{s}^{-1}$. Auxiliary surfaces parameters: $\xi_i = 0{\cdot}8152$; $\xi_o = 1{\cdot}1848$. Incident wave field amplitude for P-waves: $U_{12} = 1$ for $\theta_0 = 0$ (vertical incidence) and $U_{12} = -\sin(\theta_0)$ for $\theta_0 \neq 0$; for SV-waves: $U_{14} = 1$ for $\theta_0 = 0$ (vertical incidence) and $U_{14} = \cos(\theta_0)$ for $\theta_0 \neq 0$

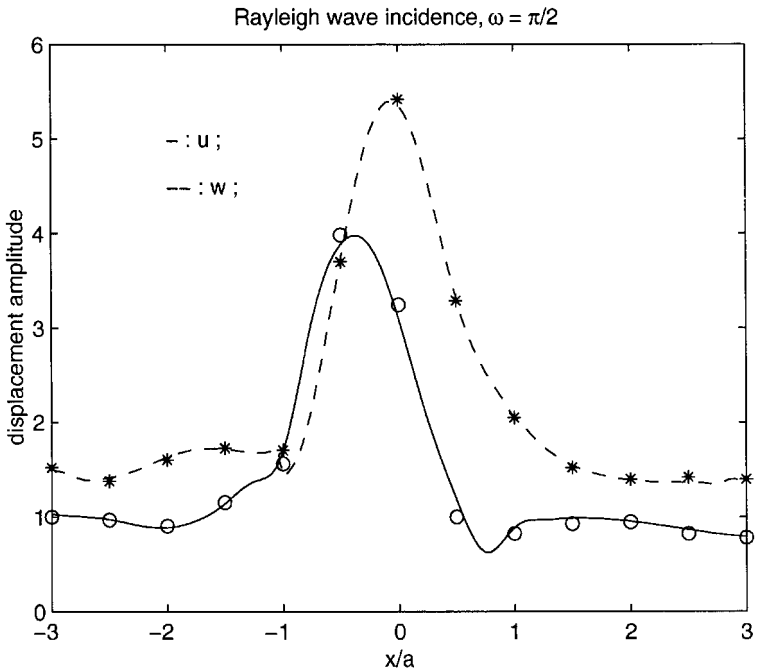

Figure 5. The same as in Figure. 4 but for incident plane harmonic Rayleigh wave. Incident wave field amplitudes: $U_{11} = 2{\cdot}3$

The inner and outer sources are placed along the surfaces $C^{(1)}$ and $C^{(2)}$, respectively, defined by

$$C^{(1)}: \begin{cases} x = R_{1\mathrm{i}} \cos\theta \\ z = R_{3\mathrm{i}} \sin\theta, \quad 0 \leqslant \theta \leqslant \pi \end{cases} \tag{38}$$

$$C^{(2)}: \begin{cases} x = R_{1\mathrm{o}} \cos\theta \\ z = R_{3\mathrm{o}} \sin\theta, \quad 0 \leqslant \theta \leqslant \pi \end{cases} \tag{39}$$

with the principal axes being defined by

$$\begin{cases} R_{1,3\mathrm{i}} = \xi_{\mathrm{i}} R_{1,3} \\ R_{1,3\mathrm{o}} = \xi_{\mathrm{o}} R_{1,3}; \quad 0 < \xi_{\mathrm{i}} < 1; \ 1 < \xi_{\mathrm{o}} \end{cases} \tag{40}$$

Here the parameters ξ_{i} and ξ_{o} are determined according to equations (33)–(36).

Therefore, if the incident wave length is given, then ds can be chosen according to equation (33) and all other parameters can be determined in accordance with relations equations (34)–(36). Since the spacing ds depends on the number of collocation points N, the key problem is to determine N.

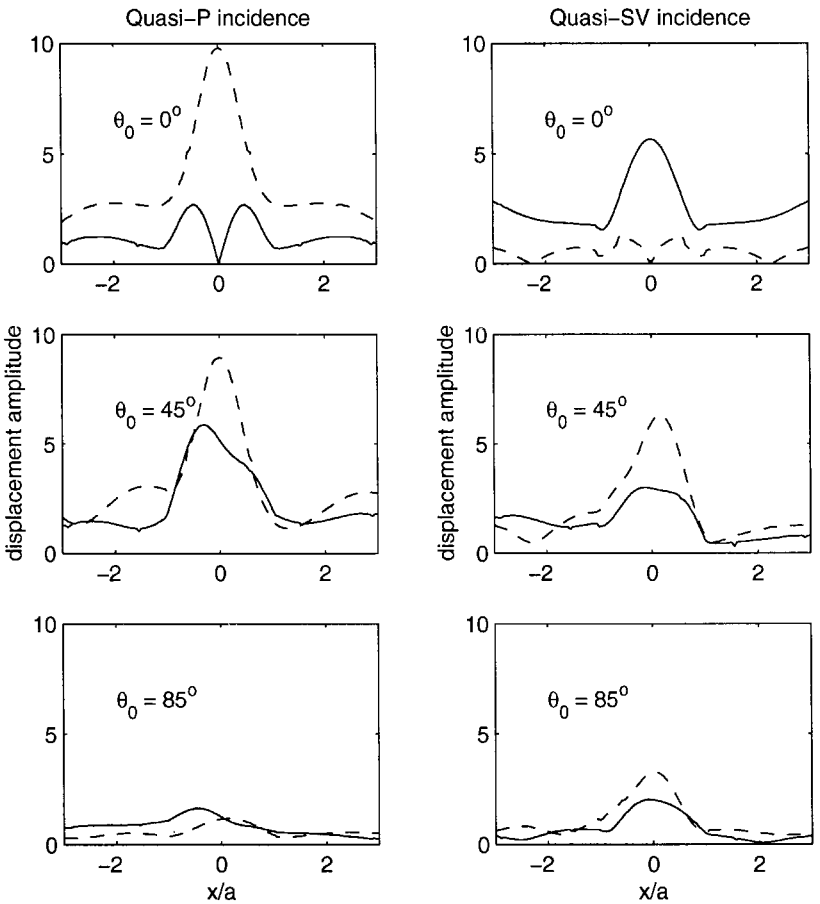

Figure 6. Surface displacement spectral amplitudes for an orthotropic semicircular basin (model 2) subjected to incident oblique incident pseudo P- and S-waves. $\omega = \pi/2\,\mathrm{s}^{-1}, N = 60, M = L = 24, N_s = 121$. Incident wave field amplitudes are the same as in Figure 4

Lack of analytical solutions for the problem at hand requires that the verification of the numerical calculations is done indirectly. This is accomplished in two different ways.

First, the so-called transparency test is performed where the material properties of the half-space and the basin are assumed to be the same. The surface response should be that of the free-field. This test allows estimation of the initial parameters, such as the orders of expansion and the number of collocation points. For the sake of briefness the results of this test are omitted. Second, the isotropic response test is performed in which the materials of the basin and the half-space are assumed to be isotropic. These results can be compared with the ones obtained for isotropic media which have been confirmed by several independent studies. Figure 4 depicts the results of isotropic response test for a semi-circular basin subjected to a vertical plane harmonic P and SV waves while Figure 5 shows the same test for an incident Rayleigh wave. The results of isotropic response test show very good agreement with those of Dravinski

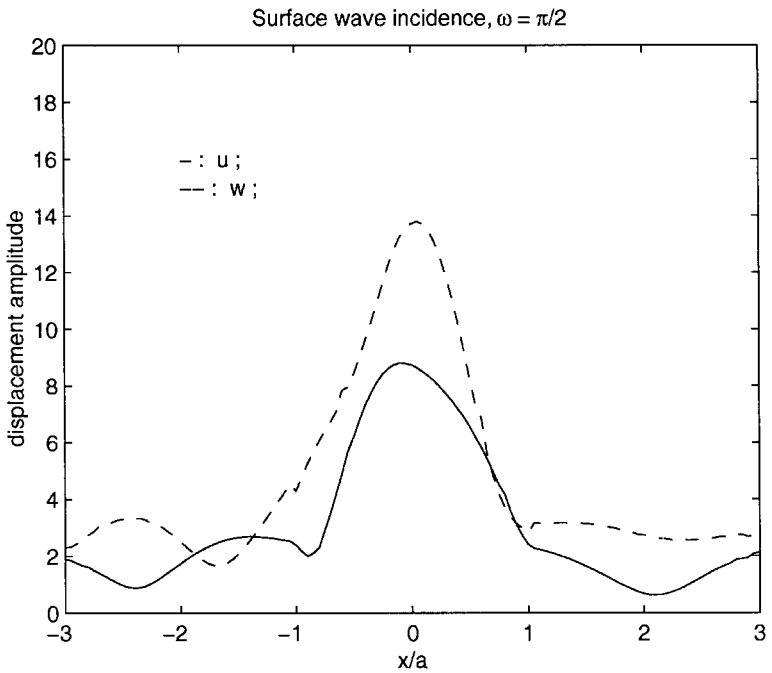

Figure 7. Surface displacement spectral amplitudes for an orthotropic semicircular basin (model 2) subjected to an incident pseudo Rayleigh wave. $\omega = \pi/2\ \mathrm{s}^{-1}, N = 60, M = L = 24, N_s = 121$. Incident wave field amplitude the same as in Figure 5

and Mossessian[7] which offers further credibility in the numerical result obtained in the present study.

4.5. Steady-state response

Surface displacement spectral amplitudes for a semi-circular basin (model 2) and incident pseudo P- and S-waves are depicted by Figure 6. For the same basin and incident pseudo Rayleigh waves the displacement spectra are shown by Figure 7. Finally, the results corresponding to a semi-elliptical basin (model 3) are shown by Figure 8. Apparently, the surface motion is very sensitive upon the type of incident wave, angle of incidence, location of observation station, and shape of the basin. In addition, the resulting ground motion strongly depends upon the frequency of the incident wave field (not shown here). Comparison of the response for orthotropic and isotropic basins (Figures 6 and 7 with Figures 4 and 5) shows that material anisotropy may cause significant change in the amplification on the surface ground motion. This is especially pronounced for the peak amplitude of the ground motion for incident pseudo P- and Rayleigh waves where anisotropic basin produced considerable larger amplification than in the case of the isotropic basin.

Therefore, presented results demonstrate the importance of anisotropy of basin in amplification of surface ground motion.

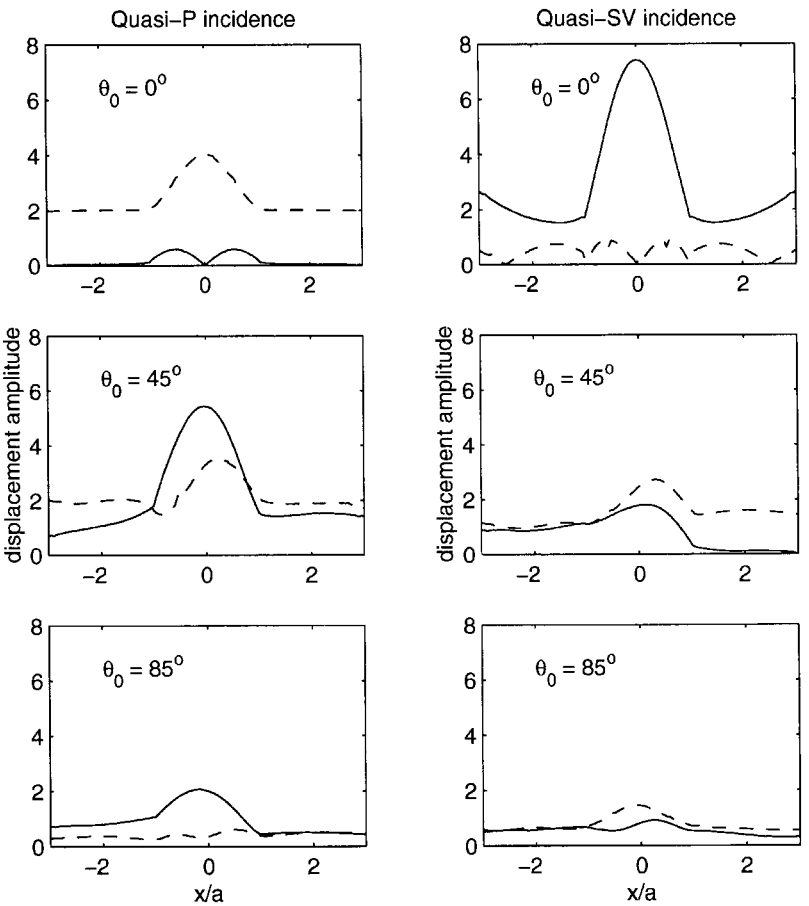

Figure 8. Surface displacement spectral amplitudes for an orthotropic semi-elliptical basin (model 3) subjected to incident oblique incident pseudo P- and S-waves. $\omega = \pi/2\,\mathrm{s}^{-1}, N = 60, M = L = 24, N_s = 121$. Incident wave field amplitudes are the same as in Figure 4

5. SUMMARY AND CONCLUSIONS

Scattering of waves in sagittal plane by an orthotropic basin of arbitrary shape has been formulated in terms of an indirect boundary integral equation approach. The known free-fields were outlined for incident pseudo P-, S-, and Rayleigh plane harmonic incidence. The unknown scattered wave field is expressed in terms of single layer potentials which involve line load half-space Green's functions and unknown density functions. The Green's functions were evaluated numerically by using adaptive Newton–Cotes or Filon quadratures. The unknown density functions are determined in the least-square sense.

Numerical results for steady-state surface response were presented for three models: model 1 which consists of a semi-circular isotropic basin and models 2 and 3 which incorporate semi-circular and semi-elliptical orthotropic basins, respectively.

Detailed testing and convergence analysis of the method was presented. Subsequently, surface response was evaluated for incident pseudo P-, S-, and Rayleigh waves. These were compared with the ones corresponding to the isotropic basin response. The results demonstrated that surface ground motion amplification strongly depends upon the nature of incident wave, shape and material properties of the basin and the half-space, and the location of the observation point. In addition it was shown that material anisotropy may significantly change surface ground motion when compared to the corresponding isotropic case.

APPENDIX I: FREE-FIELD

A.1. General plane waves

According to Nayfeh,[3] a bulk plane wave propagating in an anisotropic medium can be represented in the form

$$u_i(\mathbf{x},\omega) = U_i e^{\sqrt{-1}(\mathbf{k}\bullet\mathbf{x}-\omega t)} = U_i e^{\sqrt{-1}(k\mathbf{n}\bullet\mathbf{x}-\omega t)}, \quad i=1,2,3 \tag{41}$$

where U_i denotes displacement amplitude vector components, $\mathbf{k}=(k_1,k_2,k_3)$ is the vector wavenumber of magnitude k, and $\mathbf{n}$ is unit vector defining the direction of propagation. Substituting equation (41) into equations of motion (6)–(8) leads to the eigenvalue problem

$$(\Lambda_{il} - v^2\delta_{il})U_l = 0 \tag{42}$$

where $v=\omega/k$ is the phase velocity along $\mathbf{n}$, and

$$\Lambda_{il} = \frac{1}{\rho} c_{ijkl} n_k n_j \tag{43}$$

Existence of a non-trivial solution of equation (42) requires that

$$\det(\mathbf{\Lambda} - v^2\mathbf{I}) = 0 \tag{44}$$

Due to decoupled nature of equations of motion, equation (44) can be solved for the phase velocities in the x_1x_3-plane v_q^2, $q=1,3$ and corresponding eigenvectors $\mathbf{U}_q$. For an orthotropic material the eigenvalues are found to be

$$v_1^2 = \frac{A}{2\rho} + \frac{\sqrt{B}}{2\rho} \tag{45}$$

$$v_3^2 = \frac{A}{2\rho} - \frac{\sqrt{B}}{2\rho} \tag{46}$$

$$A = (C_{11}+C_{55})n_1^2 + (C_{33}+C_{55})n_3^2 \tag{47}$$

$$B = (C_{11}-C_{55})^2 n_1^4 + (C_{55}-C_{33})^2 n_3^4 \tag{48}$$

$$+ 2[(C_{13}+C_{55})(2C_{13}+C_{55}) \tag{49}$$

$$+ C_{55}(C_{11}+C_{13}+C_{33}) - C_{11}C_{33}]n_1^2 n_3^2 \tag{50}$$

Phase velocities v_1 correspond to pseudo P-waves and v_3 to pseudo S-waves. The eigenvectors $\mathbf{U}_q$ lead to the polarization directions

$$(1, 0, r_q)/\sqrt{1 + r_q{}^2}, \quad q = 1, 3 \tag{51}$$

where

$$\begin{aligned} r_q &= U_{3q}/U_{1q} \\ &= \frac{\rho v_q^2 - (C_{11}n_1^2 + C_{55}n_3^2)}{(C_{13} + C_{55})n_1 n_3}, \quad q = 1, 3 \end{aligned} \tag{52}$$

Therefore, the phase velocity v and the polarization of the plane wave depend upon its direction of propagation $\mathbf{n}$ and the material properties c_{ijkl}.

A.2. Reflection from a free surface

In this case it is convenient to recast the equation of the plane wave in the following form:

$$u_i(\mathbf{x}, \omega) = U_i e^{\sqrt{-1}k_1(x_1 + \alpha x_3 - ct)}, \quad i = 1, 3 \tag{53}$$

where

$$\alpha = k_3/k_1 = n_3/n_1 \tag{54}$$

and

$$c = \omega/k_1 = v/n_1 \tag{55}$$

Here c denotes apparent phase velocity along the surface of the half-space and α characterizes the direction of propagation. Once an incident plane wave strikes the surface of the half-space it generates a reflected wave. Both the amplitude and direction of the reflected wave have to be determined for a particular incidence. The horizontal phase velocity of the reflected wave is known since it has to match the corresponding phase velocity of the incident wave (see equation (55)).

Substitution of equation (53) into equations of motion (equations (6) and (8)) leads to

$$A_1\alpha^4 + B_1\alpha^2 + C_1 = 0 \tag{56}$$

where

$$\begin{aligned} A_1 &= C_{33}C_{55} \\ B_1 &= C_{33}(C_{11} - \rho c^2) + C_{55}(C_{55} - \rho c^2) - (C_{13} + C_{55})^2 \\ C_1 &= (C_{11} - \rho c^2)(C_{55} - \rho c^2) \end{aligned} \tag{57}$$

Equation (56) results in four roots

$$\begin{aligned} \alpha_1 &= n_3/n_1 = -\alpha_2 \\ \alpha_3 &= |n_1/n_3|\sqrt{\frac{(C_{11} - \rho c^2)(C_{55} - \rho c^2)}{C_{33}C_{55}}} = -\alpha_4 \end{aligned} \tag{58}$$

and the general displacement field in the sagittal plane can be represented by

$$(u_1, 0, u_3) = \sum_{q=1}^{4} (1, 0, W_q) U_{1q} \mathrm{e}^{\sqrt{-1}k_1(x_1 + \alpha_q x_3 - ct)} \tag{59}$$

where

$$W_q = \frac{U_{3q}}{U_{1q}} = \frac{\rho c^2 - C_{11} - C_{55}\alpha_q^2}{(C_{11} + C_{55})\alpha_q} \tag{60}$$

Therefore, α_1 and α_3 describe the waves propagating in the positive x_3-direction while α_2 and α_4 are associated with the waves propagating in the negative x_3-direction. Corresponding traction vector is given by

$$(t_1, 0, t_3) = (\sigma_{1j}\gamma_j, 0, \sigma_{3j}\gamma_j) \tag{61}$$

where

$$(\sigma_{13}, \sigma_{11}, \sigma_{33}) = \sum_{q=1}^{4} \sqrt{-1}k_1 (D_{3q}, D_{2q}, D_{1q}) U_{1q} \mathrm{e}^{\sqrt{-1}k_1(x_1 + \alpha_q x_3 - ct)} \tag{62}$$

and

$$D_{1q} = C_{13} + C_{33}\alpha_q W_q, \quad D_{2q} = C_{11} + C_{13}\alpha_q W_q, \quad D_{3q} = C_{55}(\alpha_q + W_q) \tag{63}$$

APPENDIX II

Matrix $\mathbf{A}$ and vector $\mathbf{f}$ in equation (29) are defined as follows:

$$\mathbf{A} = \begin{bmatrix} \mathbf{G}_{11}^{(1)} & \mathbf{G}_{13}^{(1)} & -\mathbf{G}_{11}^{(2)} & -\mathbf{G}_{13}^{(2)} \\ \mathbf{G}_{31}^{(1)} & \mathbf{G}_{33}^{(1)} & -\mathbf{G}_{31}^{(2)} & -\mathbf{G}_{33}^{(2)} \\ \mathbf{X}_1^{(1)} & \mathbf{X}_3^{(1)} & -\mathbf{X}_1^{(2)} & -\mathbf{X}_3^{(2)} \\ \mathbf{Z}_1^{(1)} & \mathbf{Z}_3^{(1)} & -\mathbf{Z}_1^{(2)} & -\mathbf{Z}_3^{(2)} \end{bmatrix} \tag{64}$$

where

$$\begin{aligned}
\mathbf{G}_{ij}^{(1)} &= [G_{ij}^{(1)}(\mathbf{x}_n, \mathbf{x}_m)], \quad \mathbf{x}_n \in C, \ \mathbf{x}_m \in C^{(1)}, \\
\mathbf{G}_{ij}^{(2)} &= [G_{ij}^{(1)}(\mathbf{x}_n, \mathbf{x}_l)], \quad \mathbf{x}_n \in C, \ \mathbf{x}_l \in C^{(2)}, \\
\mathbf{X}_i^{(1)} &= [G_{11i}^{(1)}(\mathbf{x}_n, \mathbf{x}_m)\gamma_1 + G_{13i}^{(1)}(\mathbf{x}_n, \mathbf{x}_m)\gamma_3], \ \mathbf{x}_n \in C, \ \mathbf{x}_m \in C^{(1)}, \ i = 1, 3 \\
\mathbf{X}_i^{(2)} &= [G_{11i}^{(2)}(\mathbf{x}_n, \mathbf{x}_l)\gamma_1 + G_{13i}^{(2)}(\mathbf{x}_n, \mathbf{x}_l)\gamma_3], \ \mathbf{x}_n \in C, \ \mathbf{x}_l \in C^{(2)}, \ i = 1, 3 \\
\mathbf{Z}_i^{(1)} &= [G_{13i}^{(1)}(\mathbf{x}_n, \mathbf{x}_m)\gamma_1 + G_{33i}^{(1)}(\mathbf{x}_n, \mathbf{x}_m)\gamma_3], \ \mathbf{x}_n \in C, \ \mathbf{x}_m \in C^{(1)}, \ i = 1, 3 \\
\mathbf{Z}_i^{(2)} &= [G_{13i}^{(2)}(\mathbf{x}_n, \mathbf{x}_l)\gamma_1 + G_{33i}^{(2)}(\mathbf{x}_n, \mathbf{x}_l)\gamma_3], \ \mathbf{x}_n \in C, \ \mathbf{x}_l \in C^{(2)}, \ i = 1, 3 \\
& n = 1, \ldots, N, \quad m = 1, \ldots, M, \quad l = 1, \ldots, L, \quad i, j = 1, 3
\end{aligned} \tag{65}$$

Similarly,

$$\mathbf{f} = -\begin{bmatrix} \mathbf{u}^{\mathrm{ff}} \\ \mathbf{w}^{\mathrm{ff}} \\ \mathbf{t}_1^{\mathrm{ff}} \\ \mathbf{t}_3^{\mathrm{ff}} \end{bmatrix} \tag{66}$$

where

$$\mathbf{u}^{\mathrm{ff}} = \left[\sum_{q=2,4} U_{1q}^{\mathrm{i}} \mathrm{e}^{\sqrt{-1}k_1(x_{1n}+\alpha_q x_{3n}-ct)} + \sum_{q=1,3} U_{1q}^{\mathrm{r}} \mathrm{e}^{\sqrt{-1}k_1(x_{1n}+\alpha_q x_{3n}-ct)} \right] \tag{67}$$

$$\mathbf{w}^{\mathrm{ff}} = \left[\sum_{q=2,4} U_{1q}^{i} W_q \mathrm{e}^{\sqrt{-1}k_1(x_{1n}+\alpha_q x_{3n}-ct)} + \sum_{q=1,3} U_{1q}^{\mathrm{r}} W_q \mathrm{e}^{\sqrt{-1}k_1(x_{1n}+\alpha_q x_{3n}-ct)} \right]$$

$$\mathbf{t}_1^{\mathrm{ff}} = \left[\sum_{q=2,4} \sqrt{-1}k_1(D_{2q}\gamma_1 + D_{3q}\gamma_3) U_{1q}^{\mathrm{i}} \mathrm{e}^{\sqrt{-1}k_1(x_{1n}+\alpha_q x_{3n}-ct)} \right.$$

$$\left. + \sum_{q=1,3} \sqrt{-1}k_1(D_{2q}\gamma_1 + D_{3q}\gamma_3) U_{1q}^{\mathrm{r}} \mathrm{e}^{\sqrt{-1}k_1(x_{1n}+\alpha_q x_{3n}-ct)} \right]$$

$$\mathbf{t}_3^{\mathrm{ff}} = \left[\sum_{q=2,4} \sqrt{-1}k_1(D_{3q}\gamma_1 + D_{1q}\gamma_3) U_{1q}^{\mathrm{i}} \mathrm{e}^{\sqrt{-1}k_1(x_{1n}+\alpha_q x_{3n}-ct)} \right.$$

$$\left. + \sum_{q=1,3} \sqrt{-1}k_1(D_{3q}\gamma_1 + D_{1q}\gamma_3) U_{1q}^{\mathrm{r}} \mathrm{e}^{\sqrt{-1}k_1(x_{1n}+\alpha_q x_{3n}-ct)} \right]$$

$$(x_1, 0, x_3)_n \in C, \quad n = 1, \ldots, N \tag{68}$$

ACKNOWLEDGEMENTS

The support to T. Zheng from All University Predoctoral Merit Fellowship and Teaching Assistantship at University of Southern California is greatly appreciated.

REFERENCES

1. D. E. Beskos, 'Boundary element method in dynamic analysis', *Appl. Mech. Rev.* **40**(1), 1–23 (1987).
2. M. Bouchon and O. Coutant, 'Calculation of synthetic seismograms in a laterally varying medium by the boundary element – discrete wavenumber method', *Bull. Seism. Soc. Am.* **84**, 1869–1881 (1994).
3. A. H. Nayfeh, *Wave Propagation in Layered Anisotropic Media*, Elsevier, Amsterdam, 1995.
4. R. K. N. D. Rajapakse and D. Gross, 'Transient response of an orthotropic elastic meduim with a cavity', *Wave Motion* **21**, 231–252 (1995).
5. H. Karabulut and J. F. Ferguson, 'SH wave propagation by descrete wavenumber boundary integral modeling in transversely isotropic medium', *Bull. Seism. Soc. Am.* **86**(2), 524–529 (1996).
6. T. Zheng and M. Dravinski, 'Amplification of SH waves by an orthotropic sedimentary basin', *Earthquake. Engng. Struct. Dyn.* **27**, 243–257 (1998).
7. M. Dravinski and T. K. Mossessian, 'Scattering of plane harmonic P, SV, and Rayleigh waves by dipping layers of arbitrary shape', *Bull. Seism. Soc. Am.* **77**, 212–235 (1987).
8. F. J. Sanchez-Sesma, J. Ramos-Martinez and M. Campillo, 'An indirect boundary element method applied to simulate the seismic response of alluvial valleys for incident P, S and Rayleigh waves', *Earthquake Engng. Struct. Dyn.* **22**, 279–295 (1993).
9. F. Ursell, 'On the exterior problems of acoustics', *Proc. Cambridge Phil. Soc.* **74**, 117–125 (1973).

10. V. D. Kupradze, 'Dynamical problems in elasticity', in I. N. Sneddon and R. Hill (eds), *Progress in Solid Mechanics*, Vol. 3, North-Holland, Amsterdam, 1963.
11. F. J. Sanchez-Sesma and E. Rosenblueth, 'Ground motions of canyons of arbitrary shapes under incident SHwaves', *Earthquake Engng. Struct. Dyn.* **7**, 441 (1979).
12. H. L. Wong, 'Diffraction of P, SV, and Rayleigh waves by surface topographies', *Bull. Seism. Soc. Am.* **72**, 1167–1184 (1982).
13. M. Dravinski, 'Scattering of plane harmonic SH waves by dipping layers of arbitrary shape', *Bull. Seism. Soc. Am.* **73**, 1303–1319 (1983).
14. R. K. N. D. Rajapakse and Y. Wang, 'Elastodynamic Green's functions of orthotropic half plane', *J. Engng. Mech.* **117**, 588–604 (1991).
15. A. Bjorck, *Numerical Methods for Least Squares Problems*, SIAM, Philadelphia, 1996.
16. J. E. Luco and R. J. Apsel, 'On the Green's functions for a layered half-space', *Bull. Seism. Soc. Am.* **73**, 909–929 (1983).
17. C. F. Van Loan, *Introduction to Scientific Computing*, Prentice Hall, New Jersey, 1997.
18. L. N. G. Filon, 'On a quadrature formula for trigonometric integrals', *Proc. Roy. Soc. Edin.* **49**, 38–47 (1928).
19. G. Ding and M. Dravinski, 'Scattering of SH waves in multilayered media with irregular interfaces', *Earthquake Engng. Struct. Dyn.* **25**, 1391–1404 (1996).

